MTHFD2 promotes esophageal squamous cell carcinoma progression via m6A modification-mediated upregulation and modulation of the PEBP1-RAF1 interaction

HUIJUN ZHOU[1,2*], HAN GONG[3*], XIAOHUI ZENG[2], CHONG ZENG[4], DIAN LIU[5], JIE LIU[6] and YINGYING ZHANG[7,8]

[1]Department of Gastroenterology and Urology, The Affiliated Cancer Hospital of Xiangya School of Medicine, Central South University/Hunan Cancer Hospital, Changsha, Hunan 410013, P.R. China; [2]Department of Oncology, Hunan Institute of Schistosomiasis Control/The Third Hospital of Hunan Province, Yueyang, Hunan 414000, P.R. China; [3]School of Life Sciences, Hunan Province Key Laboratory of Basic and Applied Hematology, Central South University, Changsha, Hunan 410011, P.R. China; [4]Department of Respiratory and Critical Care Medicine, The Seventh Affiliated Hospital, Hengyang Medical School, University of South China, Changsha, Hunan 410119, P.R. China; [5]Department of Lymphoma and Abdominal Radiotherapy, The Affiliated Cancer Hospital of Xiangya School of Medicine, Central South University/Hunan Cancer Hospital, Changsha, Hunan 410013, P.R. China; [6]Department of Pathology, The Affiliated Changsha Central Hospital, Hengyang Medical School, University of South China, Changsha, Hunan 410004, P.R. China; [7]Department of Oncology, Xiangya Hospital of Central South University, Changsha, Hunan 410078, P.R. China; [8]National Clinical Research Center for Geriatric Disorders, Xiangya Hospital, Central South University, Changsha, Hunan 410008, P.R. China

Received October 17, 2024; Accepted February 4, 2025

DOI: 10.3892/ijmm.2025.5509

Abstract. One-carbon metabolism plays an important role in cancer progression. Methylenetetrahydrofolate dehydrogenase 2 (MTHFD2), a mitochondrial enzyme in one-carbon metabolism, is dysregulated in several cancer types. However, the precise role and mechanisms of MTHFD2 in esophageal squamous cell carcinoma (ESCC) remain unclear. The present study unravels the multifaceted mechanisms by which MTHFD2 contributes to ESCC pathogenesis. Bioinformatics analyses revealed significant upregulation of MTHFD2 in ESCC tumor tissues, which was associated with advanced disease stage and poor patient prognosis. Validating these findings in clinical samples, MTHFD2 overexpression was confirmed through immunohistochemistry, Reverse transcription-quantitative PCR and western blotting. Knockdown of MTHFD2 inhibited ESCC cell viability, colony formation, invasion, and tumor growth *in vivo,* indicating its oncogenic potential. Mechanistically, the present study elucidated a novel regulatory axis involving N6-methyladenosine modification and MTHFD2 mRNA stability. Specifically, methyltransferase-like 3 (METTL3) and insulin-like growth factor 2 mRNA binding protein 2 (IGF2BP2) were identified as key mediators of m6A-dependent stabilization of MTHFD2 mRNA, contributing to its elevated expression in ESCC. Furthermore, MTHFD2 was found to activate PI3K/AKT and ERK signaling pathways by modulating interaction between phosphatidylethanolamine-binding protein 1 (PEBP1) and raf-1 proto-oncogene (RAF1). This modulation was achieved through direct binding of MTHFD2 to PEBP1, disrupting the inhibitory effect of PEBP1 on RAF1 and promoting downstream pathway activation. The oncogenic functions of MTHFD2 were attenuated upon PEBP1 knockdown, underscoring the role of the MTHFD2-PEBP1 axis in ESCC progression. In summary, the present study uncovers a novel regulatory mechanism involving m6A modification and the MTHFD2-PEBP1 axis, unveiling potential therapeutic avenues for targeting MTHFD2 in ESCC.

Correspondence to: Professor Yingying Zhang, Department of Oncology, Xiangya Hospital of Central South University, 172 Tongzipo Road, Changsha, Hunan 410078, P.R. China
E-mail: csuzhangyingying@163.com

*Contributed equally

Key words: methylenetetrahydrofolate dehydrogenase 2, esophageal squamous cell carcinoma, m6A modification, PEBP1, PI3K/AKT pathway

Introduction

Esophageal cancer (EC) is a notable global health burden and a leading cause of cancer mortality worldwide. In 2020, an estimated 544,076 deaths were attributed to E (1). Esophageal squamous cell carcinoma (ESCC) accounts for the majority of EC cases, representing >50% of diagnoses in China (2). Despite considerable research efforts, treatment outcomes for ESCC remain poor, with median survival ~11 months, largely due to late-stage diagnosis and the lack of effective targeted

therapies (3,4). Thus, identifying molecular markers to enable early diagnosis and prognosis prediction, as well as discovering novel therapeutic targets, is key for improving patient outcomes.

Aberrant energy metabolism is a hallmark of cancer that supports tumor growth and progression (5). Increasing evidence suggests that overactivity of one-carbon metabolism drives tumorigenesis and is associated with epigenetic regulation of cells (6,7). Methylenetetrahydrofolate dehydrogenase 2 (MTHFD2), a mitochondrial enzyme involved in one-carbon metabolism, serves an important role in physiology and pathology (8). As a bifunctional enzyme, MTHFD2 catalyzes interconversion of folate metabolites to support biosynthetic processes, including purine synthesis. MTHFD2 expression is induced in cancer to meet increased metabolic demands, and high MTHFD2 levels promote occurrence and development of tumors (9,10). While MTHFD2 dysregulation is implicated in ovarian cancer (11), glioma (12) and lung (13) and colorectal cancer (14), its functional role and mechanisms in ESCC remain unexplored.

N6-methyladenosine (m6A) RNA methylation is a prevalent post-transcriptional modification by methyltransferase complexes, recognized by RNA-binding proteins, and removed by demethylases (15). m6A signaling regulates cancer progression (16,17). In ESCC, m6A has been shown to control processes such as proliferation, invasion and metastasis (18-20). However, different m6A regulators may confer distinct regulatory outcomes in ESCC (21).

The present study investigated the clinical value and functional role of one-carbon metabolism-associated genes in ESCC, with a particular focus on MTHFD2. To elucidate the regulatory mechanisms involved, the effects of key m6A regulators, methyltransferase-like 3 (METTL3) and insulin-like growth factor 2 mRNA binding protein 2 (IGF2BP2), on MTHFD2 expression were assessed. Additionally, downstream signaling pathways influenced by MTHFD2 and the impact on the phosphatidylethanolamine-binding protein 1 (PEBP1) and raf-1 proto-oncogene (RAF1) interaction was assessed. PEBP1 inhibits the RAF1/MEK/ERK pathway, which regulates key cellular processes such as survival, proliferation and apoptosis (22,23).

Materials and methods

Data acquisition and preprocessing. The Cancer Genome Atlas (TCGA)biolinks R package (24) was used to retrieve mRNA expression data (RNA-seq V2) and corresponding clinical information for 80 patients with ESCC in the TCGA-ESCA cohort from the Genomic Data Commons portal (portal.gdc.cancer.gov/) using the GDCquery function. Patients were selected based on the disease type information classified as 'Squamous Cell Neoplasms'. GSE130078, GSE53622, and GSE53624 were downloaded from the Gene Expression Omnibus (GEO) database (https://www.ncbi.nlm.nih.gov/geo/). TCGA-ESCA cohort includes patients of Asian, White and Black or African American descent. The GSE130078 cohort consists of South Korean patients, while the GSE53622 and GSE53624 cohorts include patients from China.

Differentially expressed genes and clinical relevance analyses. MTHFD2 expression levels across pan-cancer were evaluated using the TIMER 2.0 database (25). BEST tool (rookieutopia.com/app_direct/BEST/) was used to compare MTHFD2 mRNA levels between tumor and normal tissue in ESCC datasets from GEO database. BEST also analyzed the correlation between MTHFD2 expression and clinical features in ESCC using Spearman's method. Kaplan-Meier plotter website (26) was used to assess the prognostic value of MTHFD2 in ESCC.

Gene set enrichment analysis (GSEA). GSEA was performed to assess enrichment of one carbon pool by folate and PI3K/AKT signaling pathway gene sets using MSigDB databases (https://www.gsea-msigdb.org/gsea/msigdb).

Online prediction. The sequence-based RNA adenosine methylation site predictor (SRAMP; cuilab.cn/sramp) was used to identify potential m6A modification sites in MTHFD2 mRNA. Potential protein interactions of MTHFD2 were predicted using Biological General Repository for Interaction Datasets (BioGRID) (https://thebiogrid.org/).

Cell culture. ESCC cell lines, including TE1 (CVCL_1759), KYSE30, KYSE410, KYSE150 and KYSE510, and immortalized esophageal epithelial cell Het-1A, were acquired from Wuhan Pricella Biotechnology Co., Ltd. Cells were cultured in RPMI-1640 medium supplemented with 10% fetal bovine serum (Procell Life Science & Technology Co., Ltd.) in a humidified incubator at 37˚C with 5% CO_2.

RNA interference, lentivirus production and infection. Lentiviral vectors expressing short hairpin RNAs (shRNAs) targeting MTHFD2 (shRNA#1, 5'-GCCTCTTCCAGAGCATATTGA-3'; shRNA#2, 5'-GCAGTCATTGATGTGGGAATA-3') and scrambled negative control (NC; 5'-TTCTCCGAACGTGTCACGT-3') were designed and synthesized by Shanghai GeneChem Co., Ltd.. Small interfering (si)PEBP1 (5'-GTGGTCAACATGAAGGGCAAT-3') and control siNC (Table SI) were also synthesized by GeneChem. The lentivirus production and infection and siRNA transfection were performed as previously described (27). Briefly, KYSE30 and KYSE410 cells were infected with lentivirus expressing shMTHFD2 and shNC for 48 h. Following selection with puromycin (2 μg/ml) for 72 h, knockdown efficiency was confirmed by qPCR and WB analysis as aforementioned. As for siRNA transfection, a 500 μl mixture containing 10 μl of 20 μM siPEBP1/siNC and 10 μl Lipofectamine 2000 (Thermo Fisher Scientific, Inc.) was added to KYSE30 and KYSE410 cells that had been seeded in 6-well plates 24 h earlier. The medium was replaced with fresh complete medium after 6 h. The efficiency of interference was detected by WB and qPCR after 48 h.

Reverse transcription quantitative PCR (RT-qPCR). Total RNA was extracted from cells using TRIzol (Invitrogen; Thermo Fisher Scientific, Inc.) and 1 μg RNA was reverse-transcribed to cDNA using PrimeScript RT reagent kit (Takara Biotechnology Co., Ltd.). RT-qPCR was performed with SYBR Premix Ex Taq II (Takara Biotechnology Co., Ltd.) on a 7500 Real-Time PCR System (Applied Biosystems; Thermo Fisher Scientific, Inc.). The thermocycling conditions were as follows: Initial denaturation at 95˚C for 30 sec, followed by 40 cycles of

denaturation at 95˚C for 5 sec and annealing/extension at 60˚C for 30 sec. The relative expression of target genes was calculated using the 2-ΔΔCq method with GAPDH as the reference gene (28). The primers are shown in Table SI.

Western blot (WB) analysis. Western blot was performed as described previously (29) using primary antibodies against MTHFD2 (Proteintech Group, Inc.; cat. no. #12270-1-AP), METTL14 (Proteintech Group, Inc.; #26158-1-AP) and IGF2BP2 (Proteintech Group, # 11601-1-AP; all 1:1,000) followed by HRP-conjugated secondary antibodies (1:2,000; Cell Signaling Technology, Inc.).

Immunohistochemistry (IHC). A total of 80 paired clinical ESCC and adjacent normal tissue samples collected from February 2018 to September 2019 (median age, 61 years; age range, 43-76 years; 5 female and 75 male; distance, 3 cm) were obtained from the tissue bank of the First Xiangya Hospital of Central South University (Changsha, China). IHC staining was performed to evaluate the expression of MTHFD2. Tissues were fixed in 4% paraformaldehyde at room temperature for 24 h and embedded in paraffin. Then, 5-μm sections were cut and mounted on slides. Antigen retrieval was performed using citrate buffer at 95˚C for 20 min. Slides were then washed with xylene and rehydrated in a descending alcohol series. Blocking was performed with 5% BSA(cat. no. #37520, Thermo Fisher Scientific, Inc.) at 25˚C for 1 hour. Endogenous peroxidase activity was quenched with 3% hydrogen peroxide for 10 min at 25˚C. The primary antibody against MTHFD2 (#12270-1-AP; Proteintech Group, Inc.) was (1:100) and incubated at 4˚C overnight. The secondary antibody (#SA00004-2; Proteintech Group, Inc.; Biotin-conjugated) was diluted (1:200) and incubated at room temperature for 1 h. Protein localization and staining intensity were visualized using diaminobenzidine (DAB) and scored as described previously (30). Images were captured using a light microscope at 100x magnification. Image analysis was performed using ImageJ (Java 8 version, National Institutes of Health).

Methylated RNA immunoprecipitation (MeRIP)-qPCR. MeRIP was conducted using Protein A/G magnetic beads (cat. no. #Bes5203-1, BersinBio,) according to the manufacturer's protocol. In each reaction, 50-100 μg of RNA were sonicated to produce small fragments of about 100 nt in length. After precipitation and washing, the RNA fragments were dissolved in 400 microliters of IP buffer containing RNase inhibitors. The m6A antibody (1 mg/ml) was used for immunoprecipitation, with IgG (1 mg/ml) as a negative control. Immunoprecipitated complexes were washed three times with IP buffer 3 at 4˚C for 5 min each. RNA extraction involved centrifugation at 13,000 g, 4˚C for 10 min, followed by ethanol precipitation and collection at 16,000 g, 4˚C for 30 min. The complexes were isolated using a magnetic rack, and RNA was eluted with Elution Buffer and Proteinase K at 55˚C for 30 min. Immunoprecipitated RNA was purified and reverse-transcribed to cDNA, and MTHFD2 enrichment was measured using qPCR and normalized to input controls as aforementioned. Knockdown of METTL3 and IGF2BP2 was verified to assess specificity of m6A modification.

Luciferase reporter assay. A dual-luciferase reporter system assay was performed as previously described (27). For luciferase reporter construction, the MTHFD2 sequence 5'-AGC TTGGGGTAGCCACTAATTAACTACTGTGTCTTCTGT GTCACA-3') containing predicted m6A sites was amplified by PCR and cloned into the pmirGLO reporter plasmids (Promega Corporation) downstream of the luciferase reporter gene. The empty pmirGLO vector served as a control. KYSE30 and KYSE410 cells were seeded in 24-well plates ($5x10^4$ cells/well). After 24 h, cells were co-transfected at 37˚C with pmirGLO-MTHFD2 or empty vector (500 ng), *Renilla* luciferase plasmid (50 ng) for normalization and siMETTL3 or siNC (50 nM). At 48 h post-transfection, luciferase activity was measured using the Dual-Luciferase Reporter Assay System (Promega Corporation). Each experiment was performed in triplicate.

RNA stability assay. RNA stability assays were conducted as previously described (27). Briefly, ESCC cells were treated with 10 μg/ml actinomycin D (MedChemExpress; #HY-17559) for 0, 2, and 4 h. Following RNA isolation, qRT-PCR was used to assess MTHFD2 relative expression, normalized to GAPDH. mRNA half-life was then determined using linear regression analysis.

Co-immunoprecipitation (Co-IP) assay. Co-IP assays were performed to investigate protein-protein interactions. Briefly, protein was extracted from lysed ESCC cells (Pierce IP Lysis Buffer, Thermo Fisher Scientific, Inc.). Magnetic beads were added to the protein solution and incubated at 4˚C for 30 min. Following magnetic separation, the supernatant was transferred to a new tube and divided into two groups: an IgG control group and a target antibody group. The corresponding antibodies were added overnight at 4˚C with shaking. Magnetic beads (pre-washed twice with cold PBS) were then added to each protein-antibody complex and incubated for 4-6 h at 4˚C. After another magnetic separation, the supernatant was collected and heated to 100˚C for 10 min to denature the proteins. Following centrifugation and a final magnetic bead separation, the resulting supernatant was collected for WB analysis.

T7 biotin labeled RNA synthesis and RNA pulldown assay. RNA pull-down assay was performed as previously described (27). Briefly, biotin-labeled RNA probes specific to MTHFD2 mRNA were synthesized using the Ribo RNAmax-T7 Biotin Labeled RNA Synthesis kit (#C11002-2, RiboBio) following the manufacturer's protocol. An RNA pulldown experiment was then carried out with the BersinBio RNA pulldown Kit (#Bes5102, BersinBio) according to the standard method (27). Biotin-labeled RNA probes were attached to streptavidin-coated magnetic beads for 30 min at room temperature. RNA-bead conjugates were then incubated with nucleic acid-depleted lysates (Pierce IP Lysis Buffer, Thermo Fisher Scientific, Inc.) from ESCC cells for 2 h at room temperature to capture interacting proteins. The amount of lysate used per IP reaction was 0.8 ml. The amount of magnetic beads was used according to manufacturer's protocol. After incubation, the complexes were washed with protein elution buffer provided in the kit. The centrifugation steps were performed

at 5,000 g for 1 min at room temperature. The completes were captured by the magnetic beads, then eluted and identified via WB as aforementioned.

Specifically, the biotin-labeled RNA probes were attached to streptavidin-coated magnetic beads at room temperature for 30 min. These RNA-bead conjugates were incubated with nucleic acid-depleted lysates from ESCC cells at room temperature for 2 h to capture interacting proteins. The captured proteins were subsequently eluted and identified via western blot as aforementioned.

Cell Counting Kit (CCK)-8. CCK-8 assay was employed to assess cell viability. Cells were at a density of 2,000 cells per well seeded into a 96-well plate and cultured at 37˚C. After 24, 48, 72, 96 and 120 h, CCK-8 solution (10 μl/well, Biosharp) was added, and the plate was incubated at 37˚C for 2 h. Absorbance was measured at 450 nm.

Colony formation assay. ESCC cells were seeded into 6-well plates (600 cells/well) and cultured at 37˚C for 14 days. The culture medium was changed every 3 days. Cells were fixed with 4% paraformaldehyde at 25˚C for 29 min and stained with 0.1% crystal violet at 25˚C for 20 min. Colonies (≥50 cells) were counted manually under a light microscope at x4 magnification. The experiment was repeated ≥3 times.

Transwell invasion assay. ESCC cells were seeded ($1x10^5$) in FBS-free DMEM (Thermo Fisher Scientific, Inc.) at 37˚C in the upper chamber of Matrigel-coated inserts (BD Biosciences). The Matrigel was pre-coated onto the inserts at 37˚C for 30 min. DMEM containing 15% FBS (Thermo Fisher Scientific, Inc.) was added to the lower chamber. After 24 h at 37˚C, non-invading cells on the upper membrane were removed and invading cells on the lower surface were fixed with 4% paraformaldehyde at 25˚C, stained with 0.5% crystal violet at 25˚C for 20 min and counted in five random fields of view from three independent experiments (magnification, x100).

Subcutaneous tumor formation in nude mice. KYSE30 cells with stable MTHFD2 knockdown and control cells were suspended in a 1:1 mixture of PBS and Matrigel. Six-week-old female BALB/c nude mice (n=6; Silek Jingda; weighing 20-25 g at the start of the study were subcutaneously injected with $5x10^6$ cells/mouse in the dorsal flank as previously described (31). Mice were housed in individually ventilated cages under standard conditions: 22-25˚C temperature, 50-60% humidity, 12-h light/12-h dark cycle with ad libitum access to sterile food and water. Tumor growth was monitored every 2 days and caliper measurements were taken to assess tumor volume using the formula:

$$Volume = \frac{Length \times Width^2}{2}$$

The longest diameter and maximum tumor volume measured were 1.25 cm and 0.488 cm^3 respectively. After six weeks, mice were euthanized by cervical dislocation following injection of sodium pentobarbital at a dose of 50 mg/kg (32). Humane endpoints were body temperature below 33˚C, 3 h of inactivity, and/or a weight loss exceeding 20% of the initial body weight. Death was confirmed by cessation of both respiratory and cardiac activity. Tumors were harvested for further analysis. Tumor tissues underwent IHC staining to evaluate expression levels of MTHFD2 and Ki67 as aforementioned. The present study was approved by Experimental Animal Ethics Committee of Xiangya Hospital, Central South University (approval no. XY20240407002).

Statistical analysis. All statistical analyses were conducted using R 4.2.1 (r-project.org/) or GraphPad Prism 8 (graphpad.com/). Significant differences were determined by paired Student's t-test or Wilcoxon test. One-way ANOVA followed by Tukey's post hoc test was used to evaluate differences between >2 groups. χ^2 test was used to analyze association between MTHFD2 expression and clinicopathological variables. $P<0.05$ was considered to indicate a statistically significant difference. All experiments were performed with ≥3 biological replicates. Data are presented as mean ± SD.

Results

MTHFD2 upregulation in ESCC is associated with malignant progression and poor prognosis. Activity of the one-carbon metabolism pathway was significantly enriched in tumor tissue (Fig. S1A). Differential expression analysis identified nine up- and three downregulated genes in ESCC (Fig. S1B). MTHFD2, MTHFD1L, MTHFD1 and thymidylate synthase were significantly upregulated in tumors compared with normal tissue (Figs. 1A and S1C). MTHFD2 was consistently upregulated across three independent ESCC datasets and its expression was higher in patients with higher tumor grades and metastasis (Fig. S1D-F). MTHFD2 expression across pan-cancer was upregulated in multiple tumor types (including bladder urothelial carcinoma, breast invasive carcinoma, CESC: Cervical squamous cell carcinoma and endocervical adenocarcinoma, CHOL: Cholangiocarcinoma, CRC: colorectal cancer, ESCA: Esophageal carcinoma, HNSC: Head and neck squamous cell carcinoma, kidney renal clear cell carcinoma, LIHC: Liver hepatocellular carcinoma, LUAD: Lung adenocarcinoma, LUSC: Lung squamous cell carcinoma, PCPG: Pheochromocytoma and paraganglioma, PRAD: Prostate adenocarcinoma, STAD: Stomach adenocarcinoma, THCA: Thyroid carcinoma, and UCEC: Uterine corpus endometrial carcinoma), reinforcing its role as a potential oncogene (Fig. S1F and G). Survival analysis demonstrated that high MTHFD2 expression was associated with poor recurrence-free survival (Fig. 1B).

To validate these bioinformatics findings, 80 ESCC samples were collected. IHC confirmed the elevated expression of MTHFD2 in tumor tissues (Fig. 1C and D). Kaplan-Meier analysis showed that patients with high MTHFD2 expression had worse survival outcomes (Fig. 1E). MTHFD2 expression was assessed in normal esophageal and ESCC cell lines. WB and qPCR results indicated that KYSE410 and KYSE30 cells exhibited higher MTHFD2 levels (Fig. 1F and G) and were selected for subsequent experiments.

m6A modification regulates MTHFD2 expression via METTL3-mediated mRNA stability. Considering the importance of m6A modification in the regulation of gene expression (33), it was hypothesized that upregulation of MTHFD2 is regulated by m6A modification. SRAMP

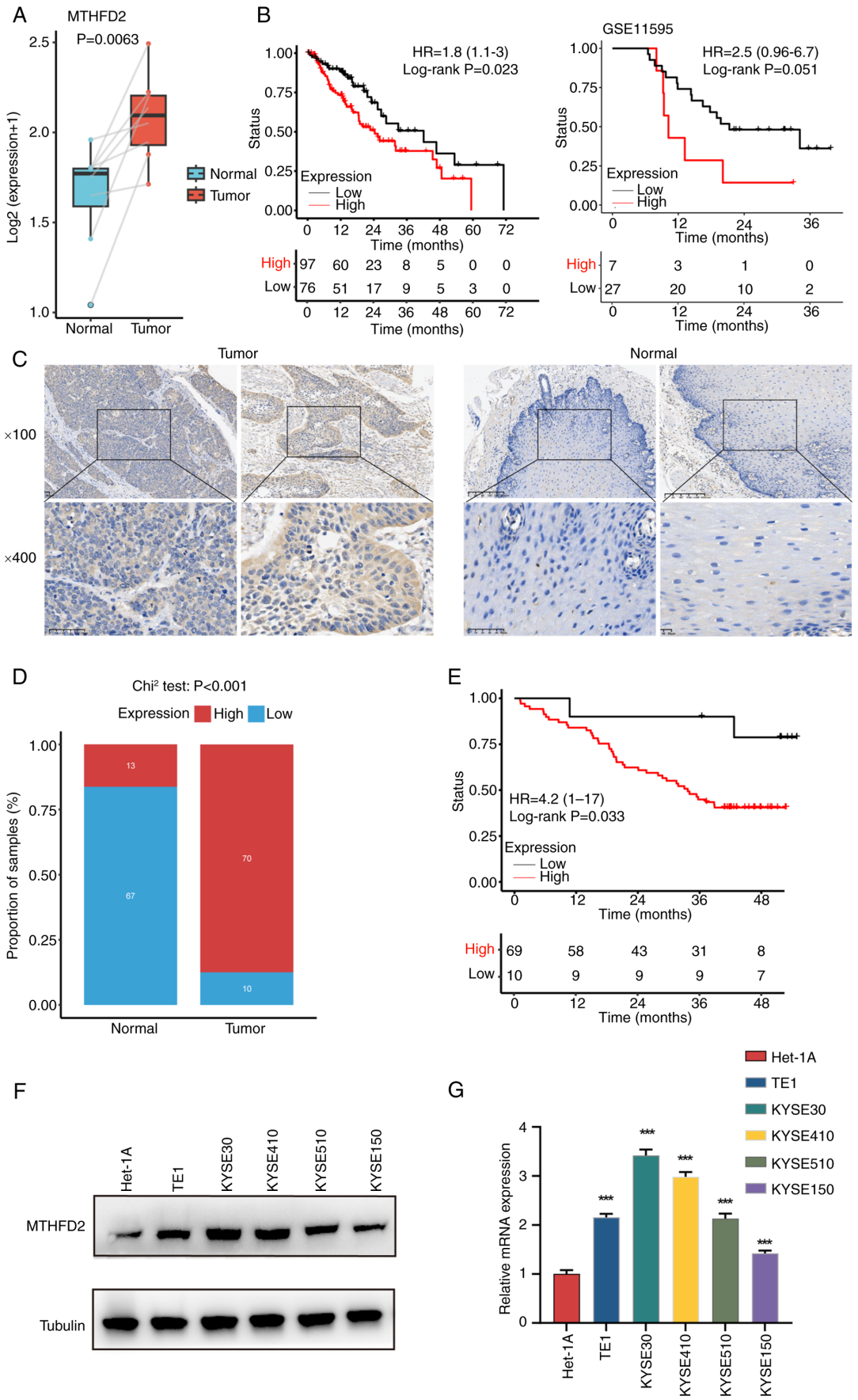

Figure 1. MTHFD2 is a potential biomarker in ESCC. (A) Expression levels of MTHFD2 in paired tumor and adjacent normal tissue samples. (B) Kaplan-Meier curves of MTHFD2 expression in The Cancer Genome Atlas-Esophageal Carcinoma and GSE11595 cohorts. (C) Immunohistochemistry analysis of MTHFD2 expression. (D) Ratio of high and low MTHFD2 expression in tumor and normal tissue. (E) Survival curves of MTHFD2 in clinical samples. (F) Western blot analysis of MTHFD2 expression in normal esophageal and ESCC cell lines. (G) Quantitative PCR analysis showing MTHFD2 expression levels in normal and ESCC cells. ***P<0.001 vs. Het-1A. ns, not significant; MTHFD2, methylenetetrahydrofolate dehydrogenase 2; ESCC, esophageal squamous cell carcinoma.

database (34) identified two high-confidence m6A modification sites on MTHFD2 (Fig. 2A). MeRIP confirmed that site 1 was modified by m6A (Fig. 2B). Further analysis revealed an association between MTHFD2 expression and 30 known m6A regulators; there were positive associations between MTHFD2 and most regulatory factors, supporting a potential regulatory role of m6A modification in MTHFD2 expression (Fig. S2A).

To explore the mechanism of m6A modification on MTHFD2, common m6A writers (METTL3, METTL16 and WTAP) were knocked down in KYSE30 and KYSE410 cells. qPCR showed that METTL3 knockdown resulted in a significant downregulation of MTHFD2 mRNA, while METTL16 and WTAP knockdown did not have a similar effect (Figs. 2C and S2B). To validate this, cells were transfected with additional METTL3-targeting sequence. WB and qPCR confirmed effective knockdown of METTL3 expression with the two sequences. (Fig. 2D and E). The RNA stability assay revealed that METTL3 knockdown led to decreased stability of MTHFD2 mRNA (Fig. 2F). Dual-luciferase reporter assay demonstrated a significant reduction in luciferase activity upon METTL3 knockdown (Fig. 2G). These findings suggested that METTL3-mediated m6A modification serves a key role in regulating MTHFD2 expression by enhancing stability of its mRNA.

IGF2BP2 recognizes m6A of MTHFD2 mRNA and enhances its stability in ESCC. In addition to writers, the m6A methylation process involves readers, the main function of which is to recognize bases where m6A modification occurs (15). To identify the readers of MTHFD2, readers (IGF2BP1, IGF2BP2 and IGF2BP3) with a high association with MTHFD2 were selected. qPCR results indicated that IGF2BP1 and IGF2BP3 knockdown did not lead to a significant downregulation of MTHFD2 mRNA (Fig. S3). Furthermore, knockdown sequences for IGF2BP2 effectively decreased METTL3 expression, as confirmed by WB and qPCR (Fig. 3A and B). MeRIP-qPCR demonstrated that the m6A antibody enriched MTHFD2 mRNA and this enrichment was markedly diminished upon METTL3 knockdown (Fig. 3C). RNA stability assay revealed that IGF2BP2 knockdown reduced the stability of MTHFD2 mRNA in both KYSE30 and KYSE410 cells (Fig. 3D). Dual-luciferase reporter experiments confirmed that MTHFD2 mRNA stability decreased following IGF2BP2 knockdown (Fig. 3E). Moreover, the RNA pull-down assay showed that the biotin-labeled MTHFD2 mRNA probe specifically precipitated IGF2BP2, whereas the control antisense probe did not (Fig. 3F). These findings indicated that METTL3 and IGF2BP2 jointly regulate stability of MTHFD2 mRNA via m6A modification in ESCC.

To investigate the role of m6A modification in regulating MTHFD2, adenine at the 1,080th position of the MTHFD2 mRNA was mutated to thymine to create a mutant construct (Fig. S4A). qPCR and WB analyses revealed that after knocking down MTHFD2, overexpression of wild-type MTHFD2 restored protein expression to baseline levels, while overexpression of m6A-mutant MTHFD2 partially restored the expression (Fig. S4B and C). MeRIP-qPCR revealed significantly reduced m6A modification in mutant compared with wild-type MTHFD2 (Fig. S4D). RIP-qPCR demonstrated that this mutation substantially impaired the binding between MTHFD2 and IGF2BP2 (Fig. S4E), which was further validated by RNA pull-down experiments (Fig. S4F). mRNA stability assay showed that the mutant MTHFD2 exhibited significantly decreased stability compared with wild-type (Fig. S4G). These findings indicated that m6A modification plays a critical role in stabilizing MTHFD2 mRNA and promoting its interaction with IGF2BP2.

Knockdown of MTHFD2 inhibits ESCC progression in vitro and tumor growth in vivo. To elucidate the functional role of MTHFD2 in ESCC, stable knockdown of MTHFD2 was induced in two cell lines, KYSE30 and KYSE410. qPCR and WB experiments confirmed significant downregulation of MTHFD2 expression (Fig. 4A and B). CCK-8 assay indicated that the viability of the MTHFD2 knockdown group was notably decreased compared with that of the control group (Fig. 4C). Plate colony formation assay supported these findings, revealing a significant reduction in proliferative capacity of ESCC cells following MTHFD2 knockdown (Fig. 4E). To assess the *in vivo* implications, a nude mouse subcutaneous tumor model was constructed. Tumor growth and weight monitoring revealed smaller tumors in the MTHFD2 knockdown group compared with controls (Fig. 4F and G). IHC results corroborated these observations, indicating significant downregulation of MTHFD2 and Ki67 levels in subcutaneous tumor tissues of the shMTHFD2 compared with shNC group (Fig. 4H). These results collectively suggest an oncogenic role of MTHFD2 in ESCC progression.

MTHFD2 promotes AKT and ERK signaling pathway activation in ESCC. To analyze the potential biological behaviors of MTHFD2 in ESCC, patients in TCGA-ESCC were divided into high and low expression groups based on median MTHFD2 expression levels (cutoff value=19.03). Differential analysis identified 124 down- and 1,073 upregulated genes (Fig. 5A). Gene Set Enrichment Analysis revealed significant enrichment of the PI3K/AKT signaling pathway in the high expression group (Fig. 5B). WB experiments showed that knockdown of MTHFD2 in KYSE30 and KYSE410 cells led to a significant decrease in levels of phosphorylated AKT (p-AKT) and p-ERK, while the total levels of AKT and ERK remained unchanged (Fig. 5C).

BioGRID database (35) identified a potential interaction between MTHFD2 PEBP1 (Fig. S5). Co-immunoprecipitation (co-IP) experiments in ESCC cells confirmed that PEBP1 and MTHFD2 bind each other (Fig. 5D and E). However, MTHFD2 knockdown did not alter the protein or mRNA levels of PEBP1, as demonstrated by WB and qPCR (Fig. 5F and G). These findings suggested that MTHFD2 promoted activation of the PI3K/AKT signaling pathway in ESCC, potentially via interaction with PEBP1, without affecting PEBP1 expression.

MTHFD2 modulates PEBP1-RAF1 interaction and PI3K/AKT pathway activation. PEBP1 binds RAF1 and inhibits the RAF1/MAPK pathway (36). It was hypothesized that MTHFD2 may inhibit binding of PEBP1 to RAF1 by interacting with PEBP1. Interaction between PEBP1 and RAF1 was assessed after knocking down MTHFD2 in KYSE30 and KYSE410 cells. Co-IP showed that the interaction between PEBP1 and RAF1 was enhanced following MTHFD2 knockdown (Fig. 6A). Knocking down and

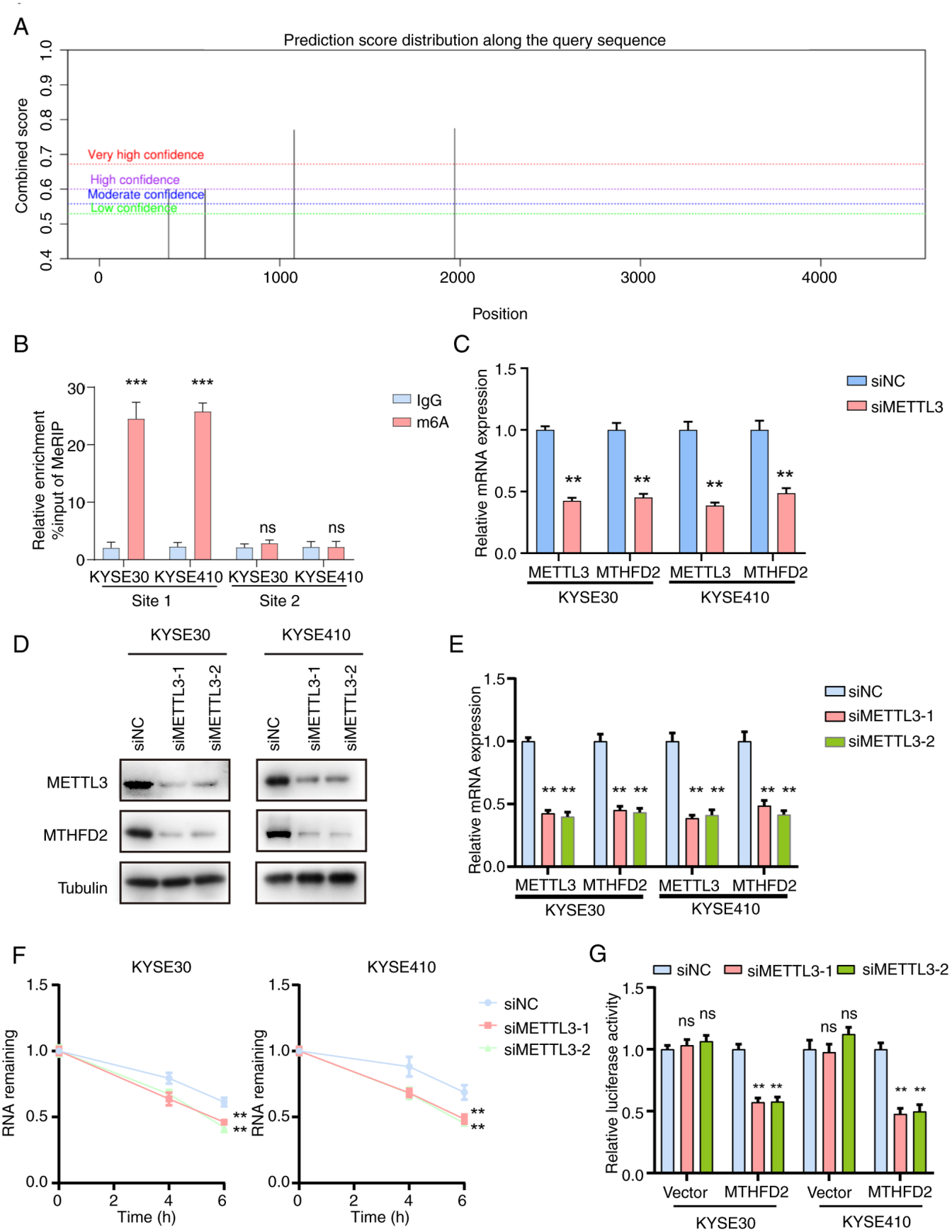

Figure 2. METTL3 regulates MTHFD2 mRNA stability. (A) Predicted m6A modification sites on MTHFD2 mRNA identified using Sequence-based RNA adenosine methylation site predictor database. (B) MeRIP confirmed the presence of m6A sites on MTHFD2 mRNA in KYSE30 and KYSE410 cells. METTL3 knockdown decreased (C) METTL3 mRNA and (D) MTHFD2 protein expression. (E) Quantitative PCR analysis of MTHFD2 expression following METTL3 knockdown. (F) RNA stability and (G) dual-luciferase reporter assay demonstrated decreased MTHFD2 mRNA stability upon METTL3 knockdown. **P<0.01, ***P<0.001 vs. siNC. ns, not significant; METTL3, methyltransferase-like 3; MTHFD2, methylenetetrahydrofolate dehydrogenase 2; si, small interfering; NC, negative control; MeRIP, methylated RNA immunoprecipitation.

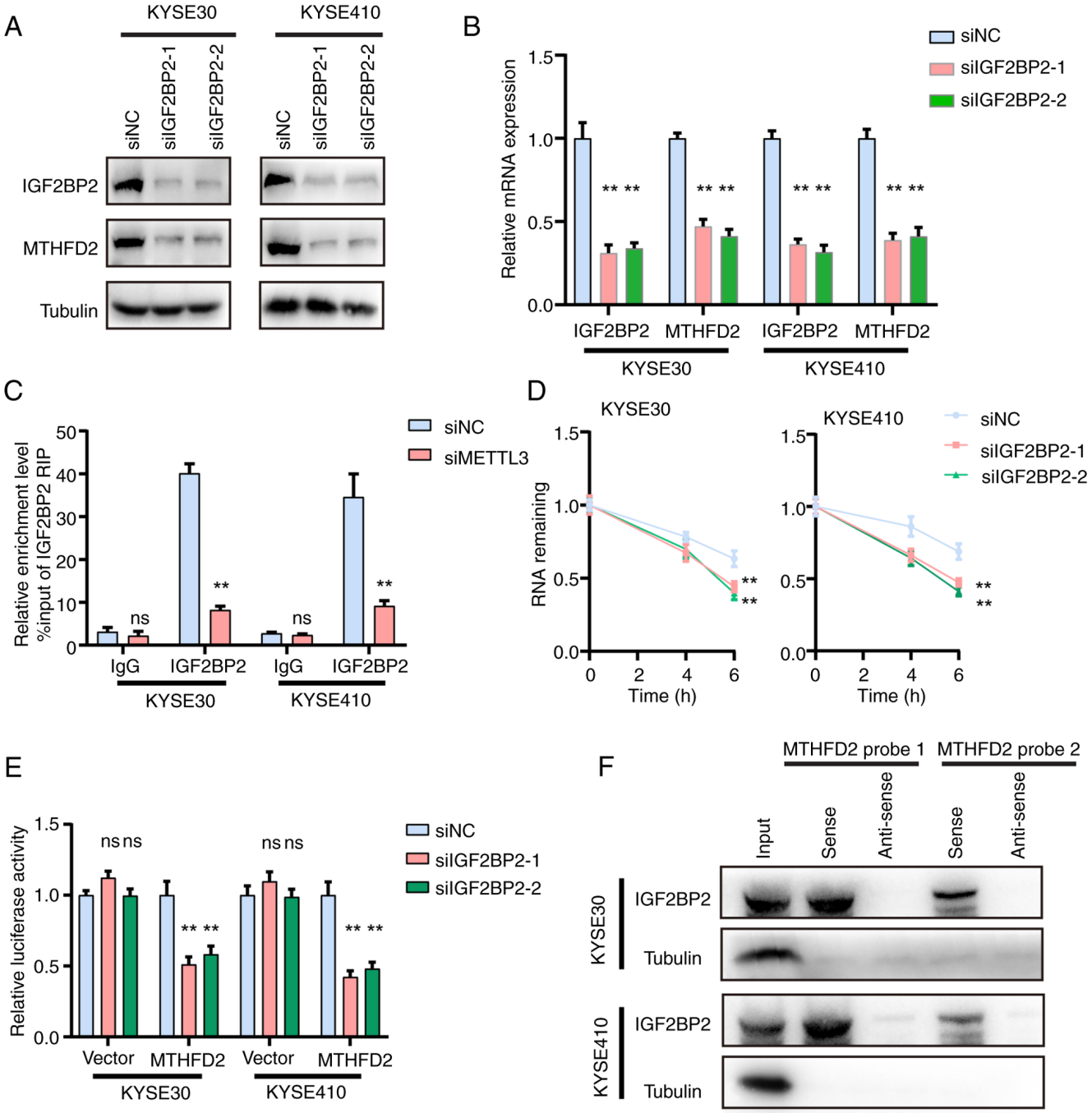

Figure 3. IGF2BP2 recognizes m6A modification on MTHFD2 mRNA. (A) Western blot analysis showed decreased MTHFD2 expression following IGF2BP2 knockdown. (B) qPCR analysis of MTHFD2 expression following IGF2BP2 knockdown in KYSE30 and KYSE410 cells. (C) Methylated RIP-qPCR demonstrating significant enrichment of MTHFD2 mRNA using m6A antibody, with this enrichment substantially reduced upon METTL3 knockdown. (D) RNA stability assay indicating reduced MTHFD2 mRNA stability following IGF2BP2 knockdown. (E) Dual-luciferase reporter assays showing decreased MTHFD2 mRNA stability following IGF2BP2 knockdown. (F) RNA pull-down assay confirmed that the biotinylated MTHFD2 mRNA probe specifically precipitated IGF2BP2. **P<0.01 vs. siNC. ns, not significant; IGF2BP, insulin-like growth factor 2 mRNA binding protein 2; MTHFD2, methylenetetrahydrofolate dehydrogenase 2; q, quantitative; RIP, RNA immunoprecipitation; m6A, N6-methyladenosine; si, small interfering; NC, negative control.

subsequently overexpressing MTHFD2 eliminated the enhanced interaction between PEBP1 and RAF1 induced by MTHFD2 knockdown (Fig. 6B) and restored the levels of p-AKT, p-ERK and p-MEK1 to wild-type levels, while the total levels of AKT, ERK, and MEK1 remained largely unchanged (Fig. 6C). These findings suggested that MTHFD2 modulated the interaction between PEBP1 and RAF1, thereby influencing activation of the PI3K/AKT signaling pathway in ESCC.

MTHFD2 exerts oncogenic functions through PEBP1 in ESCC. To confirm that MTHFD2 exerts oncogenic functions through PEBP1, MTHFD2 was knocked down followed by PEBP1. WB analysis showed that after knocking down PEBP1, the knockdown of MTHFD2 did not decrease levels of p-AKT, p-ERK and p-MEK1 (Fig. 7A). Cell viability assays using CCK-8 demonstrated that the decrease in cell viability caused by MTHFD2 knockdown was attenuated when PEBP1 was also knocked down (Fig. 7B). This was further supported by

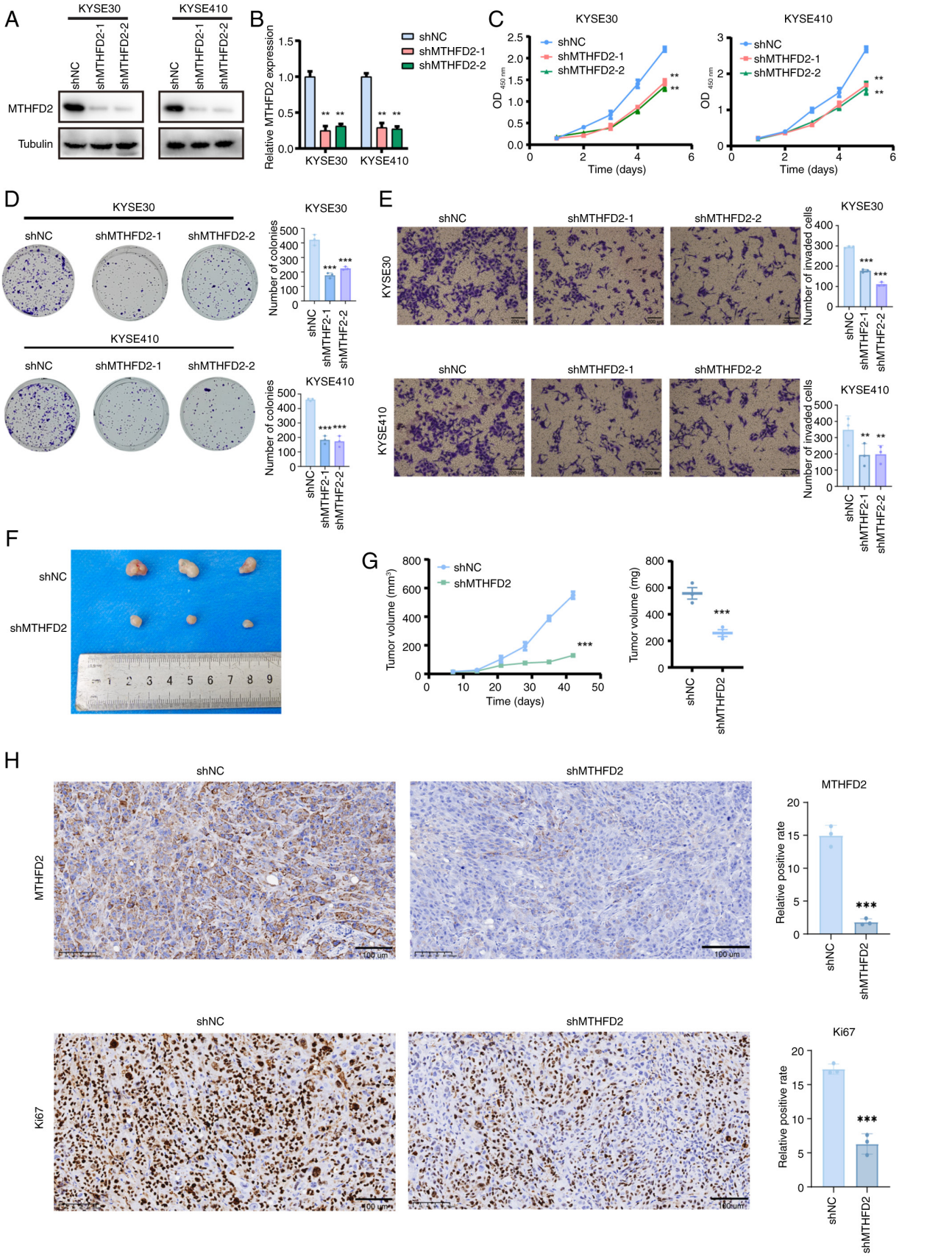

Figure 4. Knockdown of MTHFD2 inhibits esophageal squamous cell carcinoma progression both *in vitro* and *in vivo*. (A) Western blotting and (B) quantitative PCR confirmed knockdown of MTHFD2 expression in KYSE30 and KYSE410 cells. (C) MTHFD2 knockdown significantly inhibited cell viability. (D) Colony formation assays demonstrated a reduction in colony formation ability following MTHFD2 knockdown. (E) Transwell assay revealed a decrease in cell invasion following MTHFD2 knockdown. (F) *In vivo* tumor xenograft model showed decreased tumor growth in mice with shMTHFD2 tumors. (G) Tumor volume and weight. (H) Immunohistochemical analysis revealed decreased expression of MTHFD2 and Ki67 (a proliferation marker) in the shMTHFD2 group. Scale bar, 100 μm. **P<0.01, ***P<0.001 vs. shNC. ns, not significant; MTHFD2, methylenetetrahydrofolate dehydrogenase 2; sh, short hairpin; NC, negative control; OD, optical density.

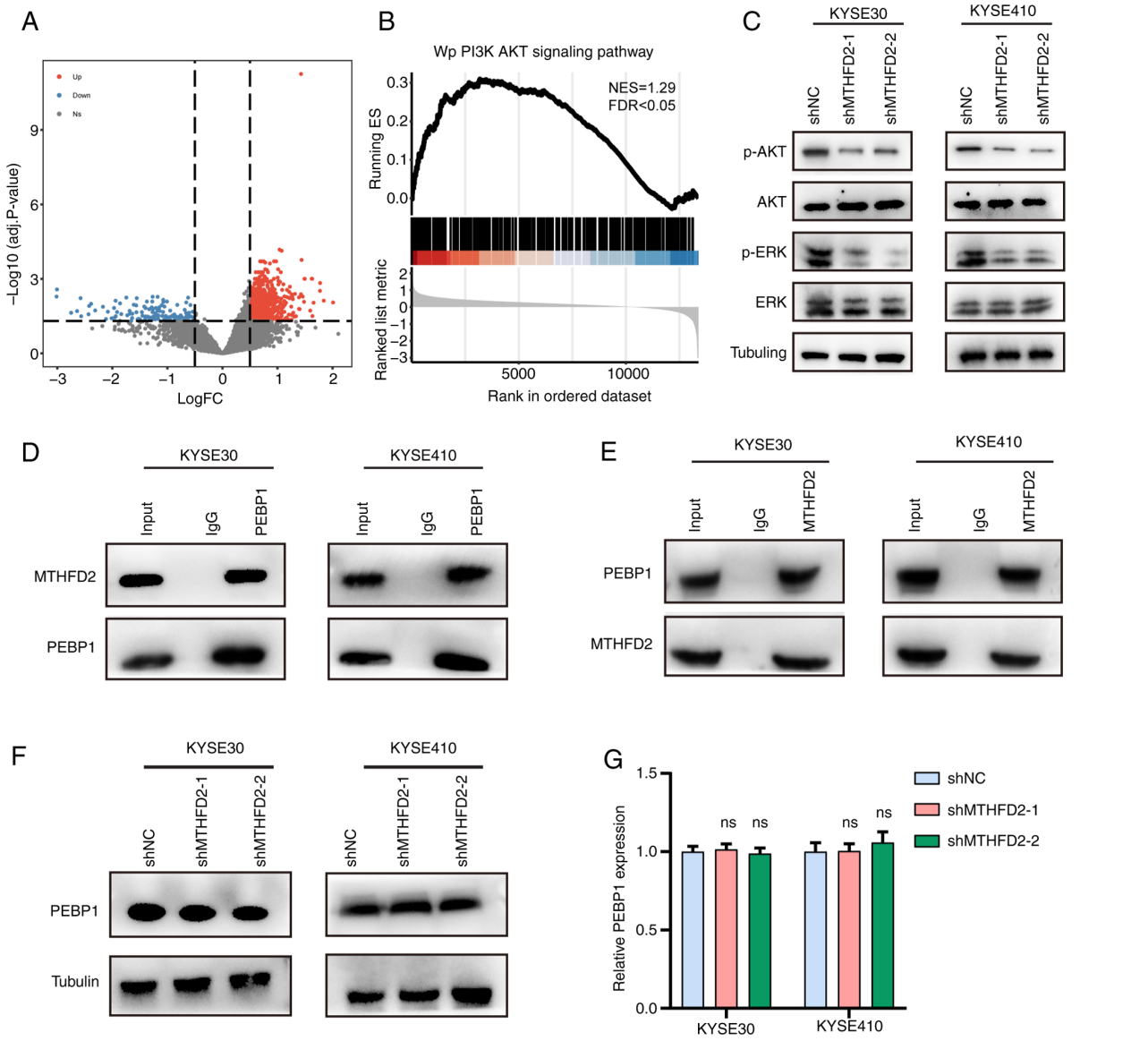

Figure 5. MTHFD2 interacts with PEBP1 and promotes AKT and ERK signaling pathway activation in esophageal squamous cell carcinoma. (A) Differentially expressed genes between patients with high and low MTHFD2 expression. (B) Gene Set Enrichment Analysis indicating enrichment of the PI3K/AKT signaling pathway in the high-MTHFD2 group. (C) Western blot analysis following MTHFD2 knockdown in KYSE30 and KYSE410 cells. Co-immunoprecipitation assay detecting the interaction between MTHFD2 and PEBP1. Immunoprecipitates were probed with (D) anti-MTHFD2 and (E) anti-PEBP1. (F) Western blot and (G) quantitative PCR showing protein and mRNA levels of PEBP1 following MTHFD2 knockdown. ns, not significant; NES, normalized enrichment score; FDR, false discovery rate; MTHFD2, methylenetetrahydrofolate dehydrogenase 2; PEBP1, phosphatidylethanolamine-binding protein 1; sh, short hairpin; NC, negative control; adj.p-value, adjusted P-value; FC, fold-change.

colony formation and Transwell assays, which confirmed that the decrease in cell viability induced by MTHFD2 knockdown was mitigated by PEBP1 knockdown (Fig. 7C and D).

As aforementioned, knockdown of MTHFD2 selectively decreased levels of p-AKT, ERK and MEK-1 without affecting the total protein levels of AKT, ERK and MEK-1. *In vivo*, IHC revealed significantly decreased levels of p-AKT, p-ERK and p-MEK1 in the MTHFD2 knockdown compared with the control group, indicating suppression of the AKT/ERK/MEK pathway in mice (Fig. 7E).

Discussion

The present study demonstrated significant upregulation of MTHFD2 in ESCC tumor tissue, which was associated with advanced pathological grade. MTHFD2 was associated with poor recurrence-free survival in patients with ESCC; this was validated in clinical samples. The proposed mechanism of action for MTHFD2-induced carcinogenic effects is summarized in Fig. 8.

He *et al* (37) identified high MTHFD2 expression in ESCC. The present study performed qPCR and WB analyses on freshly collected patient samples, providing more comprehensive validation. Furthermore, functional experiments both *in vitro* and *in vivo* suggested the potential of MTHFD2 as a biomarker in ESCC. However, clinical reliance on a single biomarker may not always provide optimal diagnostic accuracy. Combining MTHFD2 with other markers (such as proliferation marker protein Ki-67, carcinoembryonic antigen, CA19-9: carbohydrate antigen 19-9, IL6 and B-cell

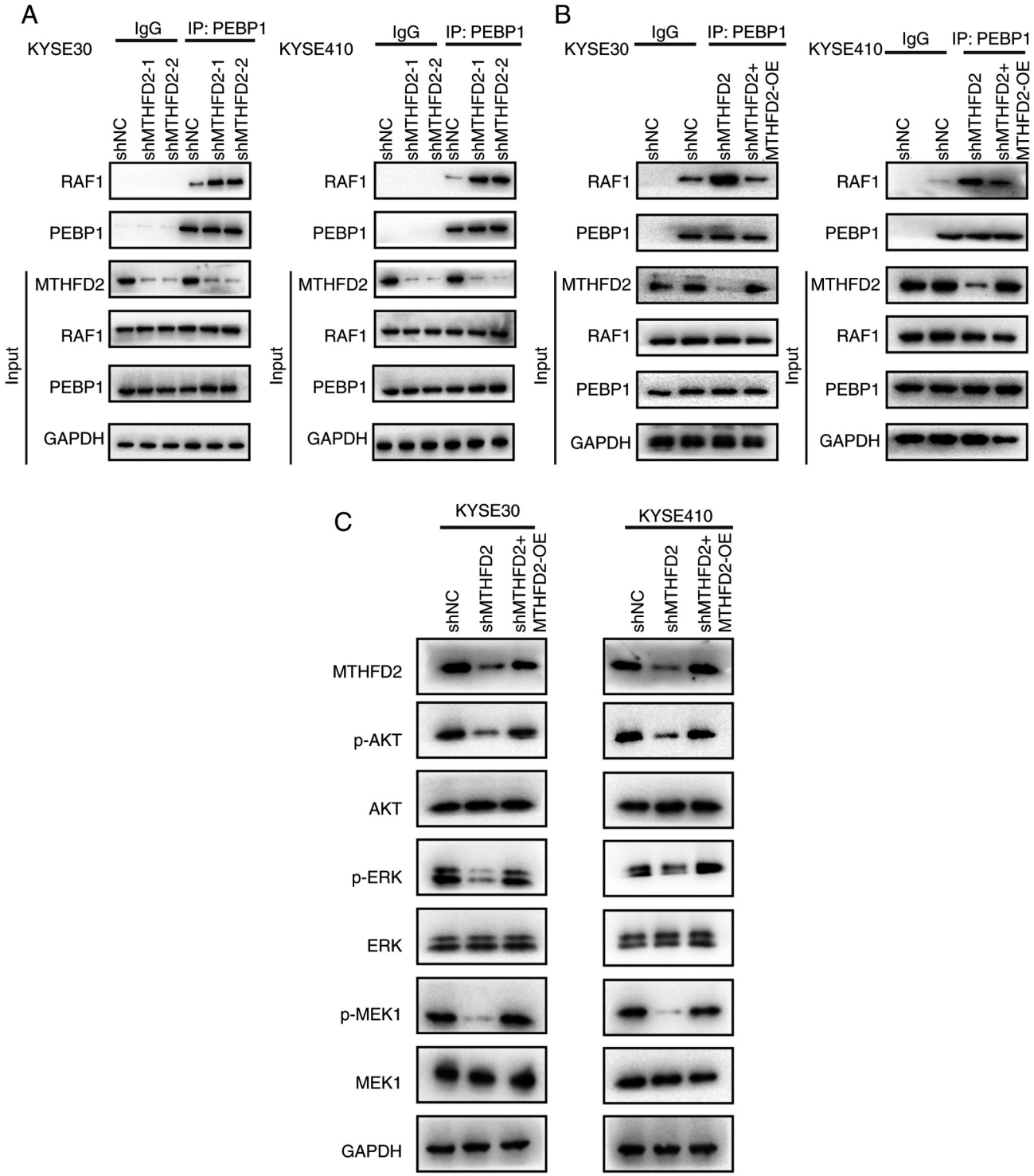

Figure 6. MTHFD2 activates the PI3K/AKT pathway by modulating PEBP1-RAF1 interaction. Co-IP detected interaction between PEBP1 and RAF1 following (A) MTHFD2 knockdown and (B) subsequent overexpression of MTHFD2. (C) Western blot analysis of the AKT/ERK/MEK signaling pathway proteins following MTHFD2 knockdown and OE. MTHFD2, methylenetetrahydrofolate dehydrogenase 2; PEBP1, phosphatidylethanolamine-binding protein 1; RAF1, raf-1 proto-oncogene; IP, immunoprecipitation; OE, overexpression; sh, short hairpin; NC, negative control; p-, phosphorylated.

lymphoma-3) (38,39) may improve the diagnostic precision for ESCC in the future.

Based on the role of m6A modification in mRNA stability and ESCC progression (18,19), it was hypothesized that m6A modification promotes high MTHFD2 expression. MeRIP-qPCR and RNA pull-down demonstrated interaction between METTL3, IGF2BP2 and MTHFD2 mRNA stabilization. Notably, the present findings align with a prior study linking IGF2BP2 with ESCC progression (40), suggesting that its functional role may rely on the stabilization of MTHFD2. This contributes to understanding of the regulatory role of m6A in ESCC.

Although previous studies have established the connection between MTHFD2 and AKT and ERK signaling

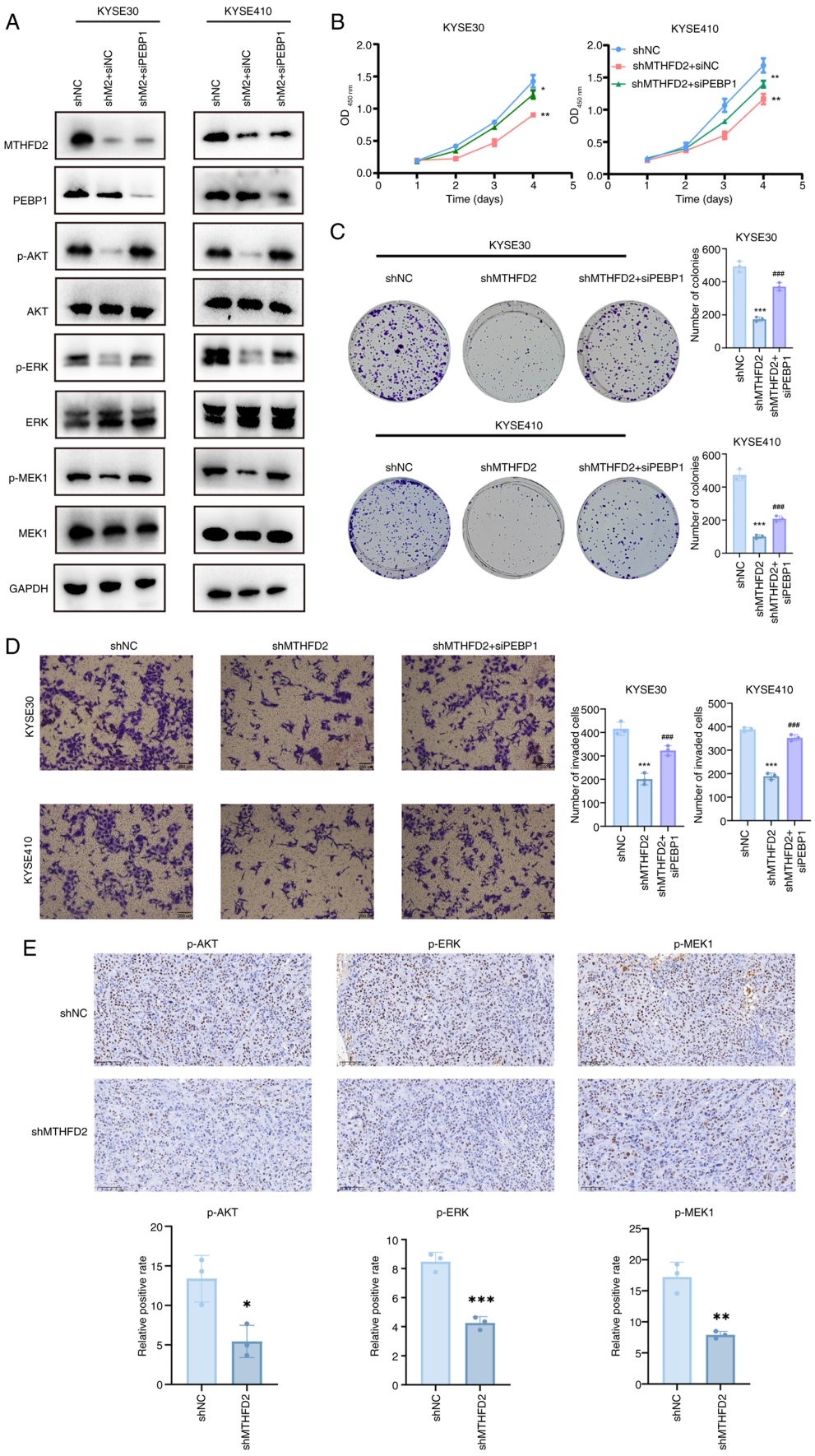

Figure 7. MTHFD2 exerts oncogenic functions via PEBP1 in esophageal squamous cell carcinoma. (A) Western blot analysis of AKT/ERK/MEK signaling pathway following MTHFD2 and PEBP1 knockdown. (B) Cell Counting Kit-8, (C) colony formation and (D) Transwell invasion assay following MTHFD2 and PEBP1 knockdown. (E) Immunohistochemical staining of p-AKT, p-ERK and p-MEK1 in mouse tumors. Scale bar, 100 μm. *P<0.05, **P<0.01, ***P<0.001 vs. shNC. $^{\#\#\#}$P<0.001 vs. shMTHFD2. MTHFD, methylenetetrahydrofolate dehydrogenase; PEBP, phosphatidylethanolamine-binding protein; p-, phosphorylated; sh, short hairpin; NC, negative control; si, small interfering; OD, optical density.

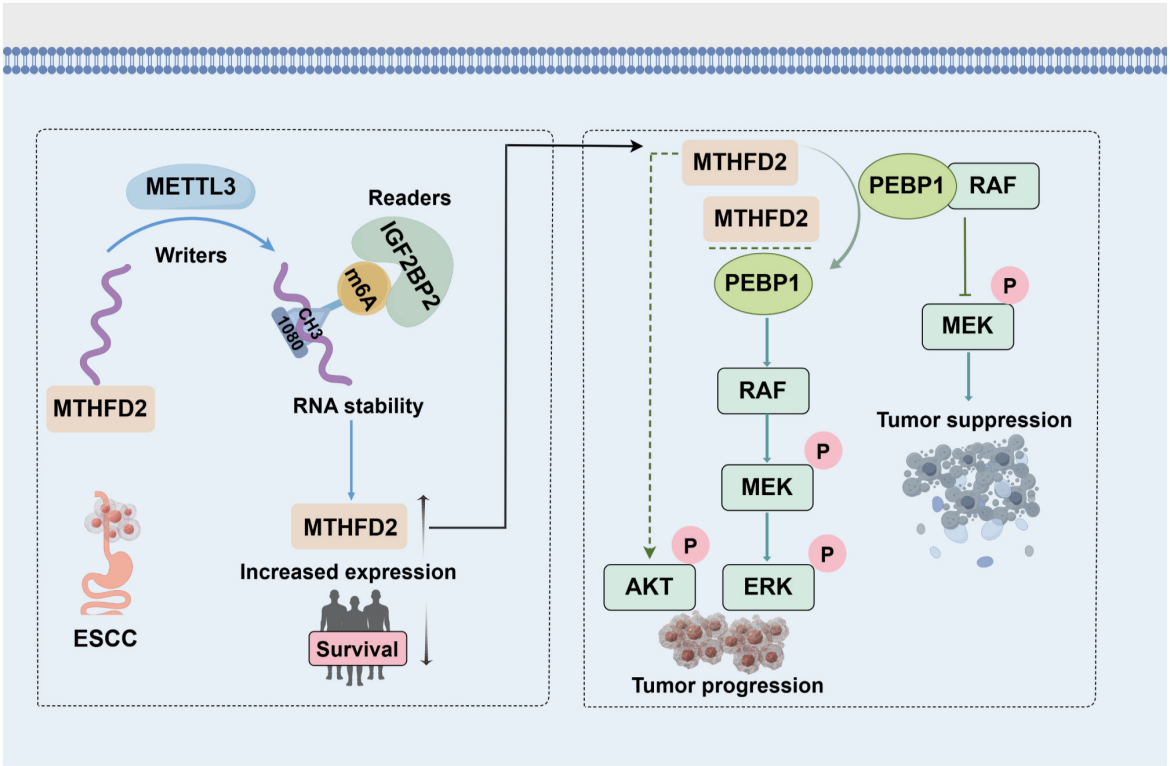

Figure 8. Mechanism by which m6A modification-mediated MTHFD2 upregulation drives tumor-promoting effects via the PEBP1-RAF1/MEK/ERK signaling cascade. METTL3 and IGF2BP2, which collaboratively induce m6A modification at position 1,080 of MTHFD2 mRNA, enhancing its stability and expression. Elevated MTHFD2 levels correlate with poor prognosis in ESCC patients. Mechanistically, MTHFD2 interacts with PEBP1, disrupting PEBP1's interaction with RAF1 and consequently activating the RAF1/MEK/ERK pathway. ESCC, esophageal squamous cell carcinoma; MTHFD2, methylenetetrahydrofolate dehydrogenase 2; METTL3, methyltransferase-like 3; IGF2BP2, insulin-like growth factor 2 mRNA binding protein 2; PEBP1, phosphatidylethanolamine-binding protein 1; RAF, Raf-1 proto-oncogene; MEK, mitogen-activated protein kinase kinase 1; ERK, mitogen-activated protein kinase 1.

pathways (41-44), the mechanism by which MTHFD2 regulates these pathways remains unclear. After knocking down MTHFD2 in KYSE30 and KYSE410 cells, Co-IP showed that the interaction between PEBP1 and RAF1 was enhanced. In addition, knocking down and subsequently overexpressing MTHFD2 abolished the enhanced interaction between PEBP1 and RAF1 induced by MTHFD2 knockdown. The levels of downstream key effectors p-AKT, p-ERK and p-MEK1 were also restored to wild-type levels. The present results suggested that MTHFD2 may inhibit PEBP1 binding to RAF1 in a competitive binding manner. However, the specific region of interaction between MTHFD2 and PEBP1 warrants further investigation to elucidate how MTHFD2 regulates PEBP1-RAF1 interaction.

Given the role of MTHFD2 in tumorigenesis (41,45-47), it may serve as a promising therapeutic target in ESCC. Targeting MTHFD2 may allow modulation of the PEBP1-RAF1 signaling axis, potentially overcoming resistance to conventional therapy. Preclinical studies have demonstrated the efficacy of small molecule MTHFD2 inhibitors in disrupting cancer cell proliferation across various tumor types, including glioblastoma and non-small cell lung cancer, and breast cancer (48-50), suggesting a similar therapeutic potential in ESCC. Further preclinical studies, including *in vivo* models of ESCC, and subsequent clinical trials are necessary to evaluate the safety, efficacy and optimal therapeutic regimen for MTHFD2-targeted intervention.

Cancer immunotherapy, particularly immune checkpoint inhibitors, has reshaped the treatment landscape for cancer (51). However, a limited number of patients responds to immunotherapy, highlighting the need for investigation into the tumor microenvironment and development of alternative immunotherapeutic strategies. Studies have revealed that MTHFD2 upregulates PD-L1 expression, thereby facilitating immune evasion (52,53). Furthermore, MTHFD2 is implicated in regulation of macrophage polarization and T cell function, both of which are key for the immune response (54,55). As immune checkpoint molecules such as programmed cell death protein 1 and PD-L1 are increasingly used in immunotherapy (56,57), MTHFD2 could serve not only as a prognostic biomarker but also as a potential therapeutic target.

The present study has limitations. MTHFD2, as a single biomarker, may not capture the full complexity of ESCC progression. Integrating MTHFD2 with other biomarkers may enhance prognostic accuracy. Larger patient cohorts are key for external validation and future research should investigate additional regulatory mechanisms affecting MTHFD2 expression in ESCC.

In conclusion, the present study contributes to understanding ESCC pathogenesis by highlighting the role of MTHFD2 and its regulation in disrupting the suppression of RAF1 by PEBP1. The present results may facilitate further investigation into the intricate biology of ESCC and the potential therapeutic implications of targeting MTHFD2.

Acknowledgements

Not applicable.

Funding

The present study was supported by the Hunan Provincial Health High Level Talent Support Program (grant no. 20240304103), Key Research and Development Program of Hunan Province (grant no. 2024JK2108), Wu Jieping Medical Foundation Research Special Fund (grant no. 320.6750.2023-19-30), Natural Science Foundation of Hunan Province, China (grant nos. 2022JJ40251 and 2022JJ30985), 'Love Lung' Tumor Treatment Clinical Scientific Research Innovation Public Welfare Project (grant no. AF008), Health Research Project of Hunan Provincial Health Commission (grant no. W20243220).

Availability of data and materials

The data generated in the present study may be requested from the corresponding author.

Authors' contributions

YZ conceived the study, designed the experiments and revised the manuscript. HZ and HG performed the experiments, analyzed the data and wrote the manuscript. XZ and CZ performed the experiments. DL and JL analyzed the data. All authors have read and approved the final manuscript. HZ and YZ confirm the authenticity of all the raw data.

Ethics approval and consent to participate

The present study was performed according to the ethical guidelines of the Helsinki Declaration and approved by the institutional review board of Xiangya Hospital of Central South University (approval no. 2024111342). All patients provided informed written consent to participate.

Patient consent for publication

Not applicable.

Competing interests

The authors declare that they have no competing interests.

References

1. Sung H, Ferlay J, Siegel RL, Laversanne M, Soerjomataram I, Jemal A and Bray F: Global Cancer Statistics 2020: GLOBOCAN estimates of incidence and mortality worldwide for 36 cancers in 185 countries. CA Cancer J Clin 71: 209-249, 2021.
2. DaSilva LL, Aguiar PN Jr and de Lima Lopes G: Immunotherapy for advanced esophageal squamous cell carcinoma-renewed enthusiasm and a lingering challenge. JAMA Oncol 7: 1613-1614, 2021.
3. Li Y, Yang B, Ma Y, Peng X, Wang Z, Sheng B, Wei Z, Cui Y and Liu Z: Phosphoproteomics reveals therapeutic targets of esophageal squamous cell carcinoma. Signal Transduct Target Ther 6: 381, 2021.
4. Jiang K, Yin X, Zhang Q, Yin J, Tang Q, Xu M, Wu L, Shen Y, Zhou Z, Yu H and Yan S: STC2 activates PRMT5 to induce radioresistance through DNA damage repair and ferroptosis pathways in esophageal squamous cell carcinoma. Redox Biol 60: 102626, 2023.
5. Pavlova NN, Zhu J and Thompson CB: The hallmarks of cancer metabolism: Still emerging. Cell Metab 34: 355-577, 2022.
6. Locasale JW: Serine, glycine and one-carbon units: Cancer metabolism in full circle. Nat Rev Cancer 13: 572-583, 2013.
7. Pan S, Fan M, Liu Z, Li X and Wang H: Serine, glycine and one-carbon metabolism in cancer (Review). Int J Oncol 58: 158-170, 2021.
8. Ducker GS and Rabinowitz JD: One-carbon metabolism in health and disease. Cell Metab 25: 27-42, 2017.
9. Nilsson R, Jain M, Madhusudhan N, Sheppard NG, Strittmatter L, Kampf C, Huang J, Asplund A and Mootha VK: Metabolic enzyme expression highlights a key role for MTHFD2 and the mitochondrial folate pathway in cancer. Nat Commun 5: 3128, 2014.
10. Zhu Z and Leung GKK: More than a metabolic enzyme: MTHFD2 as a novel target for anticancer therapy? Front Oncol 10: 658, 2020.
11. Cui X, Su H, Yang J, Wu X, Huo K, Jing X and Zhang S: Up-regulation of MTHFD2 is associated with clinicopathological characteristics and poor survival in ovarian cancer, possibly by regulating MOB1A signaling. J Ovarian Res 15: 23, 2022.
12. Shi LF, Zhang Q, Shou XY and Niu HJ: Expression and prognostic value identification of methylenetetrahydrofolate dehydrogenase 2 (MTHFD2) in brain low-grade glioma. Int J Gen Med 14: 4517-4527, 2021.
13. Geng QQ, Wu QF, Zhang Y, Zhang GJ, Fu JK and Chen NZ: Clinical significance of circ-MTHFD2 in diagnosis, pathological staging and prognosis of NSCLC. Eur Rev Med Pharmacol Sci 24: 9473-9479.
14. Ju HQ, Lu YX, Chen DL, Zuo ZX, Liu ZX, Wu QN, Mo HY, Wang ZX, Wang DS, Pu HY, *et al*: Modulation of redox homeostasis by inhibition of MTHFD2 in colorectal cancer: Mechanisms and therapeutic implications. J Natl Cancer Inst 111: 584-596, 2019.
15. An Y and Duan H: The role of m6A RNA methylation in cancer metabolism. Mol Cancer 21: 14, 2022.
16. Liu T, Wei Q, Jin J, Luo Q, Liu Y, Yang Y, Cheng C, Li L, Pi J, Si Y, *et al*: The m6A reader YTHDF1 promotes ovarian cancer progression via augmenting EIF3C translation. Nucleic Acids Res 48: 3816-3831, 2020.
17. Zeng C, Huang W, Li Y and Weng H: Roles of METTL3 in cancer: Mechanisms and therapeutic targeting. J Hematol Oncol 13: 117, 2020.
18. Cui Y, Zhang C, Ma S, Li Z, Wang W, Li Y, Ma Y, Fang J, Wang Y, Cao W and Guan F: RNA m6A demethylase FTO-mediated epigenetic up-regulation of LINC00022 promotes tumorigenesis in esophageal squamous cell carcinoma. J Exp Clin Cancer Res 40: 294, 2021.
19. Wang W, Shao F, Yang X, Wang J, Zhu R, Yang Y, Zhao G, Guo D, Sun Y, Wang J, *et al*: METTL3 promotes tumour development by decreasing APC expression mediated by APC mRNA N(6)-methyladenosine-dependent YTHDF binding. Nat Commun 12: 3803, 2021.
20. Zhao Y, Li Y, Zhu R, Feng R, Cui H, Yu X, Huang F, Zhang R, Chen X, Li L, *et al*: RPS15 interacted with IGF2BP1 to promote esophageal squamous cell carcinoma development via recognizing m^{6}A modification. Signal Transduct Target Ther 8: 224, 2023.
21. Li Y, Niu C, Wang N, Huang X, Cao S, Cui S, Chen T, Huo X and Zhou R: The role of m^{6}A modification and m^{6}A regulators in esophageal cancer. Cancers (Basel) 14: 5139, 2022.
22. Qi ZH, Xu HX, Zhang SR, Xu JZ, Li S, Gao HL, Jin W, Wang WQ, Wu CT, Ni QX, *et al*: RIPK4/PEBP1 axis promotes pancreatic cancer cell migration and invasion by activating RAF1/MEK/ERK signaling. Int J Oncol 52: 1105-1116, 2018.
23. Yang X, Wang Y, Lu P, Shen Y, Zhao X, Zhu Y, Jiang Z, Yang H, Pan H, Zhao L, *et al*: PEBP1 suppresses HIV transcription and induces latency by inactivating MAPK/NF-kappaB signaling. EMBO Rep 21: e49305, 2020.
24. Colaprico A, Silva TC, Olsen C, Garofano L, Cava C, Garolini D, Sabedot TS, Malta TM, Pagnotta SM, Castiglioni I, *et al*: TCGAbiolinks: An R/bioconductor package for integrative analysis of TCGA data. Nucleic Acids Res 44: e71, 2016.
25. Li T, Fan J, Wang B, Traugh N, Chen Q, Liu JS, Li B and Liu XS: TIMER: A web server for comprehensive analysis of tumor-infiltrating immune cells. Cancer Res 77: e108-e110, 2017.
26. Nagy A, Munkacsy G and Gyorffy B: Pancancer survival analysis of cancer hallmark genes. Sci Rep 11: 6047, 2021.

27. Zhou H, Zeng C, Liu J, Luo H and Huang W: F-box protein 43, stabilized by N6-methyladenosine methylation, enhances hepatocellular carcinoma cell growth and invasion via promoting p53 degradation in a ubiquitin conjugating enzyme E2 c-dependent manner. Cancers (Basel) 15: 957, 2023.
28. Livak KJ and Schmittgen TD: Analysis of relative gene expression data using real-time quantitative PCR and the 2(-Delta Delta C(T)) method. Methods 25: 402-408, 2001.
29. Yang Q, Zhu W and Gong H: Subtype classification based on T cell proliferation-related regulator genes and risk model for predicting outcomes of lung adenocarcinoma. Front Immunol 14: 1148483, 2023.
30. Zhang P, Li H, Gong H, Tian Y, Chen F, Li X, Xie C, Tu C, Qian S, Tan Y, *et al*: c-Myc-XRCC2-FOS axis promotes the proliferation and the resistance to doxorubicin of NSCLC. Biomed Pharmacother 179: 117315, 2024.
31. Song L, Gong H, Lin C, Wang C, Liu L, Wu J, Li M and Li J: Flotillin-1 promotes tumor necrosis factor-alpha receptor signaling and activation of NF-kappaB in esophageal squamous cell carcinoma cells. Gastroenterology 143: 995-1005.e12, 2012.
32. Carbone L, Carbone ET, Yi EM, Bauer DB, Lindstrom KA, Parker JM, Austin JA, Seo Y, Gandhi AD and Wilkerson JD: Assessing cervical dislocation as a humane euthanasia method in mice. J Am Assoc Lab Anim Sci 51: 352-356, 2012.
33. Sendinc E and Shi Y: RNA m6A methylation across the transcriptome. Mol Cell 83: 428-441, 2023.
34. Zhou Y, Zeng P, Li YH, Zhang Z and Cui Q: SRAMP: Prediction of mammalian N6-methyladenosine (m6A) sites based on sequence-derived features. Nucleic Acids Res 44: e91, 2016.
35. Oughtred R, Stark C, Breitkreutz BJ, Rust J, Boucher L, Chang C, Kolas N, O'Donnell L, Leung G, McAdam R, *et al*: The BioGRID interaction database: 2019 update. Nucleic Acids Res 47: D529-D41, 2019.
36. Abd Alla J and Quitterer U: The RAF kinase inhibitor protein (RKIP): Good as tumour suppressor, bad for the heart. Cells 11: 654, 2022.
37. He H, Li PC, Jia W, Hu B and Ji CS: High expression of methylenetetrahydrofolate dehydrogenase 2 (MTHFD2) in esophageal squamous cell carcinoma and its clinical prognostic significance. Med Sci Monit 26: e920259, 2020.
38. Soares-Lima SC, Gonzaga IM, Camuzi D, Nicolau-Neto P, Vieira da Silva R, Guaraldi S, Ferreira MA, Hernandez-Vargas H, Herceg Z and Ribeiro Pinto LF: IL6 and BCL3 expression are potential biomarkers in esophageal squamous cell carcinoma. Front Oncol 11: 722417, 2021.
39. Yang Y, Huang X, Zhou L, Deng T, Ning T, Liu R, Zhang L, Bai M, Zhang H, Li H and Ba Y: Clinical use of tumor biomarkers in prediction for prognosis and chemotherapeutic effect in esophageal squamous cell carcinoma. BMC Cancer 19: 526, 2019.
40. Lu F, Chen W, Jiang T, Cheng C, Wang B, Lu Z, Huang G, Qiu J, Wei W, Yang M and Huang X: Expression profile, clinical significance and biological functions of IGF2BP2 in esophageal squamous cell carcinoma. Exp Ther Med 23: 252, 2022.
41. Shi Y, Xu Y, Yao J, Yan C, Su H, Zhang X, Chen E and Ying K: MTHFD2 promotes tumorigenesis and metastasis in lung adenocarcinoma by regulating AKT/GSK-3beta/beta-catenin signalling. J Cell Mol Med 25: 7013-7027, 2021.
42. Deng X, Liu X, Hu B, Liu J, Fu B and Zhang W: Upregulation of MTHFD2 is associated with PD-L1 activation in bladder cancer via the PI3K/AKT pathway. Int J Mol Med 51: 14, 2023.
43. Wu S, Cai W, Shi Z, Ming X, Yang X, Zhou Y, Chen X and Yang M: Knockdown of MTHFD2 inhibits proliferation and migration of nasopharyngeal carcinoma cells through the ERK signaling pathway. Biochem Biophys Res Commun 614: 47-55, 2022.
44. Mo X, Liu Q, Liang K and Song Y: Interference with MTHFD2 induces ferroptosis in ovarian cancer cells through ERK signaling to suppress tumor malignant progression. J Bioenerg Biomembr 56: 333-345, 2024.
45. Zhang H, Zhu S, Zhou H, Li R, Xia X and Xiong H: Identification of MTHFD2 as a prognostic biomarker and ferroptosis regulator in triple-negative breast cancer. Front Oncol 13: 1098357, 2023.
46. Mo HY, Wang RB, Ma MY, Zhang Y, Li XY, Wen WR, Han Y and Tian T: MTHFD2-mediated redox homeostasis promotes gastric cancer progression under hypoxic conditions. Redox Rep 29: 2345455, 2024.
47. Wang J, Yu Z, Jiang Y, Le T, Wu Y, Li Z, Zhang G, Wu F and Ma H: Downregulation of MTHFD2 inhibits proliferation and enhances chemosensitivity in hepatocellular carcinoma via PI3K/AKT pathway. Front Biosci (Landmark Ed) 29: 35, 2024.
48. Zhu Z, Kiang KM, Li N, Liu J, Zhang P, Jin L, He X, Zhang S and Leung GK: Folate enzyme MTHFD2 links one-carbon metabolism to unfolded protein response in glioblastoma. Cancer Lett 549: 215903, 2022.
49. Zhou F, Yuan Z, Gong Y, Li L, Wang Y, Wang X, Ma C, Yang L, Liu Z, Wang L, *et al*: Pharmacological targeting of MTHFD2 suppresses NSCLC via the regulation of ILK signaling pathway. Biomed Pharmacother 161: 114412, 2023.
50. Ramos L, Henriksson M, Helleday T and Green AC: Targeting MTHFD2 to exploit cancer-specific metabolism and the DNA damage response. Cancer Res 84: 9-16, 2024.
51. Vesely MD, Zhang T and Chen L: Resistance mechanisms to anti-PD cancer immunotherapy. Annu Rev Immunol 40: 45-74, 2022.
52. Shang M, Yang H, Yang R, Chen T, Fu Y, Li Y, Fang X, Zhang K, Zhang J, Li H, *et al*: The folate cycle enzyme MTHFD2 induces cancer immune evasion through PD-L1 up-regulation. Nat Commun 12: 1940, 2021.
53. Li L, Zhang Y, Hu W, Zou F, Ning J, Rao T, Ruan Y, Yu W and Cheng F: MTHFD2 promotes PD-L1 expression via activation of the JAK/STAT signalling pathway in bladder cancer. J Cell Mol Med 27: 2922-2936, 2023.
54. Shang M, Ni L, Shan X, Cui Y, Hu P, Ji Z, Shen L, Zhang Y, Zhou J, Chen B, *et al*: MTHFD2 reprograms macrophage polarization by inhibiting PTEN. Cell Rep 42: 112481, 2023.
55. Sugiura A, Andrejeva G, Voss K, Heintzman DR, Xu X, Madden MZ, Ye X, Beier KL, Chowdhury NU, Wolf MM, *et al*: MTHFD2 is a metabolic checkpoint controlling effector and regulatory T cell fate and function. Immunity 55: 65-81.e9, 2022.
56. Hashimoto K, Nishimura S, Ito T, Kakinoki R and Akagi M: Immunohistochemical expression and clinicopathological assessment of PD-1, PD-L1, NY-ESO-1, and MAGE-A4 expression in highly aggressive soft tissue sarcomas. Eur J Histochem 66: 3393, 2022.
57. Chu X, Tian W, Wang Z, Zhang J and Zhou R: Co-inhibition of TIGIT and PD-1/PD-L1 in cancer immunotherapy: Mechanisms and clinical trials. Mol Cancer 22: 101, 2023.